Effects of a constant electric field on the diffusional instability of cubic autocatalytic reaction fronts

J. D'Hernoncourt and A. De Wit
Nonlinear Physical Chemistry Unit, Université Libre de Bruxelles, CP 231-Campus Plaine, 1050 Brussels, Belgium and Center for Nonlinear Phenomena and Complex Systems, Université Libre de Bruxelles, CP 231-Campus Plaine, 1050 Brussels, Belgium

J. H. Merkin
Department of Applied Mathematics, University of Leeds, Leeds LS2 9JT, United Kingdom

An electric field applied in the direction of propagation of a chemical reaction-diffusion front can affect the stability of this front with regard to diffusive instabilities. The influence of an applied constant electric field is investigated by a linear stability analysis and by nonlinear simulations of a simple chemical system based on the cubic autocatalytic reaction $A^- + 2B^- \rightarrow 3B^-$. The diffusional stability of the front is seen to depend on the intensity E and sign of the applied field, and D, the ratio diffusion coefficients of the reactant species. Depending on E, the front can become more or less diffusively unstable for a given value of D. Above a critical value of E, which depends on D, electrophoretic separation of the two fronts is observed. © *2007 American Institute of Physics.*
[DOI: 10.1063/1.2566796]

I. INTRODUCTION

Autocatalytic chemical reactions are, in spatially distributed systems and under relatively unrestrictive initiation conditions, capable of sustaining propagating reaction fronts. These are self-similar structures that convert a substrate A (at some uniform concentration a_0) fully into an autocatalyst B. If the diffusion coefficients of the reactants A and B are sufficiently different, then these reaction fronts can develop diffusional instabilities. This has been clearly demonstrated for the cubic autocatalytic reaction,[1,2]

$$A + 2B \rightarrow 3B \quad \text{rate } k_0ab^2, \tag{1}$$

where a and b, are, respectively, the concentrations of A and B and k_0 is a constant. The important parameter in determining whether a diffusional instability will occur is $D = D_B/D_A$, the ratio of the diffusion coefficients of the autocatalyst D_B and substrate D_A. If $D < D_c \simeq 0.424$, a linear stability analysis shows that the reaction front is diffusionally unstable[2] (see also Ref. 3). As pointed out in Ref. 3 a, perhaps unexpected, feature of this stability analysis is that the linear growth rate has a maximum value at a nonzero value $D_0 \simeq 0.16$ of D, with the growth rate then decreasing to zero as D is decreased from D_0. In the situation when the front is unstable ($D < D_c$), a planar reaction front, perturbed slightly, initially develops into an organized cellular structure[1] and, if allowed to evolve further, irregular spatiotemporal structures are seen to arise.[2]

Reaction (1) can be used as a model for the iodate-arsenous acid (IAA) system in the arsenous acid excess case,[4] with A and B taken, respectively, to represent IO_3^- and I^-. Reaction fronts in the IAA system have been shown experimentally to develop diffusional instabilities.[5] In these experiments α-cyclodextrin was used to bind with the autocatalyst to produce the different mass transport rates for the

substrate and autocatalyst necessary for the instability. The diffusive destabilization of planar reaction fronts have also been observed in the chlorite-tetrathionate (CT) system.[6–9]

Electric fields, applied in the direction of propagation, can have a significant effect on the diffusional instability of reaction fronts. This has been shown theoretically for fronts based on reaction scheme (1) (Refs. 10 and 11) and for a model of the CT system,[12] with an experimental demonstration of the instability also being given in Ref. 12. These studies suggest that, dependent on the strength and orientation, an applied electric field can destabilize an otherwise stable configuration and, conversely, can stabilize a system that would be unstable in field-free conditions. As a consequence, applying an electric field in the direction of propagation can have substantial effects on the stability characteristics of reaction fronts.

The general derivation presented in Refs. 10 and 11 for the cubic autocatalytic reaction allows for ions with any charge, either positive or negative. Here we restrict attention to the case when the substrate and autocatalyst have the same ionic charge. This situation was considered only briefly in this previous work and hence our detailed consideration of this specific case adds to these previous results. The situation we have in mind is the IAA system in the arsenous acid excess case for which both reactants have the same (negative) charge. This reaction can be represented by, on modifying Eq. (1),

$$A^- + 2B^- \rightarrow 3B^- \quad \text{rate } k_0ab^2. \tag{2}$$
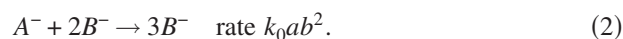
It is reaction (2) that we study. The stability analysis presented in Refs. 10 and 11 is based largely on b_s, the (dimensionless) concentration of B^- at the rear of the planar traveling front. In effect, b_s cannot be predetermined and arises out of the solution to the (planar) traveling wave equations. It
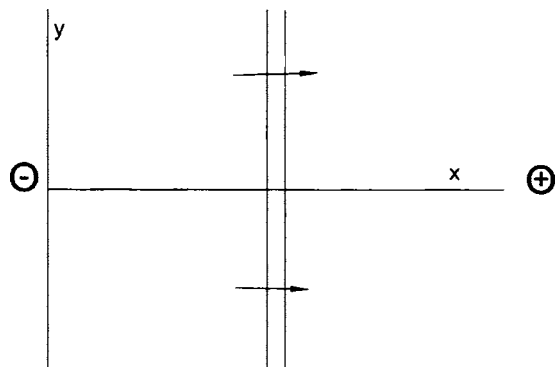
126, 104504-1

FIG. 1. Schematic representation of the system. The polarity is for the negative charged ions in Eq. (2) and for a positive value of E, with this being reversed for a negative value of E.

depends on both D and the (dimensionless) electric field strength E, which are the physical parameters that can normally be specified in an experimental setup. Thus to make our results more readily available for checking against experimental findings, we modify the approach given in Refs. 10 and 11 and here regard D and E as specifiable with b_s and the (dimensionless) wave speed c then being dependent on these parameters.

Thus the objective of this article is to study the influence of an electric field applied in the direction of propagation of a simple autocatalytic reaction-diffusion front on its diffusive instabilities. We aim at providing stability properties in a parameter space spanned by E and D. To do so, we will analyze both the changes in stability properties and nonlinear dynamics of the diffusive instabilities as a function of D and E. The structure of this article is therefore organized as follows. We start by deriving the equations for our model. We then discuss briefly the properties of the planar reaction fronts before examining the (linear) stability of these fronts. We then describe the results of our numerical simulations and finally draw some general conclusions.

II. MATHEMATICAL MODEL

Our model is based on the ionic version of the cubic autocatalytic reaction (2), which has been shown to be a good model for the IAA system for experiments conducted in the arsenous acid excess case.[4] We limit attention to two-dimensional spatial geometry, with coordinates x measuring distance in the direction of propagation and y along the (planar) reaction front. The electric field, of dimensionless strength E, is assumed to be planar, constant, and acting in the direction of propagation of the reaction front, see Fig. 1, with polarity as indicated in this figure consistent with the ionic charges in reaction (2) and a positive field strength. The resulting dimensionless equations that govern our model, on making the constant field approximation[13] and which can be derived directly from Refs. 14–16, for example, are then

$$\frac{\partial a}{\partial t} + E\frac{\partial a}{\partial x} = \left(\frac{\partial^2 a}{\partial x^2} + \frac{\partial^2 a}{\partial y^2}\right) - ab^2, \tag{3}$$

$$\frac{\partial b}{\partial t} + DE\frac{\partial b}{\partial x} = D\left(\frac{\partial^2 b}{\partial x^2} + \frac{\partial^2 b}{\partial y^2}\right) + ab^2. \tag{4}$$

To derive Eqs. (3) and (4) we scaled the concentrations on a_0, the initial (uniform) concentration of A^-, and introduced the time and length scales $T_0 = 1/k_0 a_0^2$ and $L_0 = (D_A/k_0 a_0^2)^{1/2}$. E is related to its dimensional version $\mathcal{E}$ by $E = (F/RT) \times (D_A/k_0 a_0^2)^{1/2}\mathcal{E}$ (where R and F are gas and Faraday's constants, respectively, and T is the absolute temperature, assumed constant) and $D = D_B/D_A$ is the ratio of diffusion coefficients. We assume that E can take both positive and negative values.

Initially $a = 1$ and $b = 0$ with a local (strip) input of B^-. This generates a reaction between A^- and B^-, which evolves into two, equivalent counterpropagating reaction fronts which become separated from each other as time increases. We concentrate on one of these reaction fronts, the base state for our stability analysis.

III. TRAVELING WAVES

We introduce the traveling coordinate $\zeta = x - ct$, where c is the (constant) wave speed, and look for a solution to Eqs. (3) and (4) in the form $a = a(\zeta)$, $b = b(\zeta)$. This leads to the traveling wave equations,

$$a'' + (c-E)a' - ab^2 = 0, \quad Db'' + (c-DE)b' + ab^2 = 0, \tag{5}$$

on $-\infty < \zeta < \infty$, where primes denote differentiation with respect to ζ. Equations (5) are subject to the boundary conditions,

$$a \to 1, \quad b \to 0 \quad \text{as } \zeta \to \infty, \quad a \to 0, \, b \to b_s \quad \text{as } \zeta \to -\infty, \tag{6}$$

for some constant b_s to be found. Eliminating the reaction terms, and integrating and applying the boundary conditions as $\zeta \to \infty$ give

$$a' + (c-E)a + Db' + (c-DE)b = c - E. \tag{7}$$

From relation (7), applying the boundary conditions as $\zeta \to -\infty$, we have

$$b_s = \frac{c-E}{c-DE} = 1 + \frac{(D-1)E}{c-DE}, \tag{8}$$

giving a relation for b_s, the dimensionless concentration of B^- at the rear of the wave, in terms of the wave speed c and the strength E of the electric field. Equations (5) require $(c - DE) > 0$ and so expression (8) shows that $b_s > 1$ or < 1 depending on the signs of E and $(D-1)$; $b_s = 1$ only when $E = 0$ or $D = 1$.

Equations (5) and (6) have been discussed in detail in Refs. 14 and 17. For $D > 1$, there is a negative lower bound on E for the existence of traveling wave solutions, whereas for $D < 1$ there is a positive upper bound E_c on E for existence. A graph of the wave speed c against E, obtained by solving Eqs. (5) and (6) and numerically, is shown in Fig. 2(a) for $D = 0.2$ and a graph of E_c against D is shown in Fig. 2(b). Note that E_c increases with D and appears to tend to
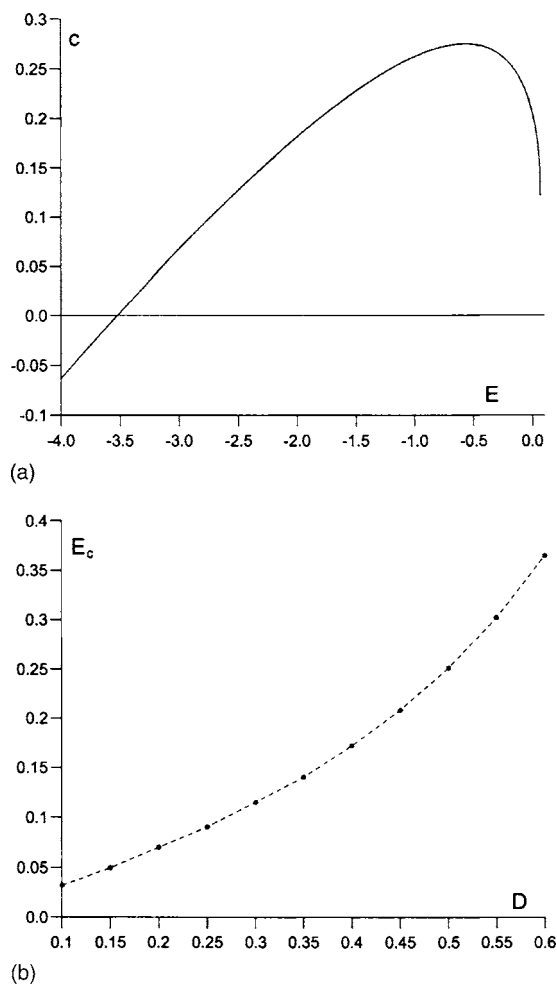
FIG. 2. (a) A graph of the wave speed c of the traveling waves against E, obtained from a numerical integration of Eqs. (5) and (6) with $D=0.2$. (b) A graph of E_c, the upper bound for the existence of traveling waves (for $D<1$), against D. Electrophoretic separation is observed for $E>E_c$ at fixed D.

FIG. 3. (a) Dispersion curves (plots of σ against k) obtained from a numerical solution of Eqs. (13) and (14), for $D=0.1$ and $E=0.0$, -0.25, -0.5, -1.0, and -1.25. (b) $\sigma_{\max}$, the maximum value of the growth rate σ, plotted against $|E|$ for $D=0.1$. Values of $\sigma_{\max}$ and $k_{\max}$ obtained from the integrations of Eqs. (3) and (4) are shown by ■.

zero as D decreases. For $D=0.2$, the upper bound for existence is $E_c=0.0698$. A point to note from Fig. 2(a) is that the wave speed first *increases* in a negative field, reaching a maximum value of $c=0.2749$ at $E=-0.568$, before falling to zero at $E=-1/\sqrt{2D}=-3.5355$, after which $c<0$ (with $E=0$, $c=0.2065$ for $D=0.2$). Results for $D=0.5$ and $D=0.1$ have been given in Refs. 14 and 17, respectively. These show qualitatively similar behavior, except that for $D=0.5$ the wave speed decreases monotonically for $E<0$. This point was discussed fully in Ref. 17. For values of the field strength E for which there are no traveling wave solutions, there is electrophoretic separation of the reacting species.[14] This results in separate concentration profiles for A^- and B^-, propagating with speeds $|E|$ and $D|E|$, respectively.

IV. LINEAR STABILITY ANALYSIS

To derive the equations for our linear stability analysis (LSA) we first write Eqs. (3) and (4) in terms of the traveling coordinate ζ (defined above). We then perturb about the traveling wave solutions $a(\zeta)$ and $b(\zeta)$ as given by Eqs. (5) and (6), setting
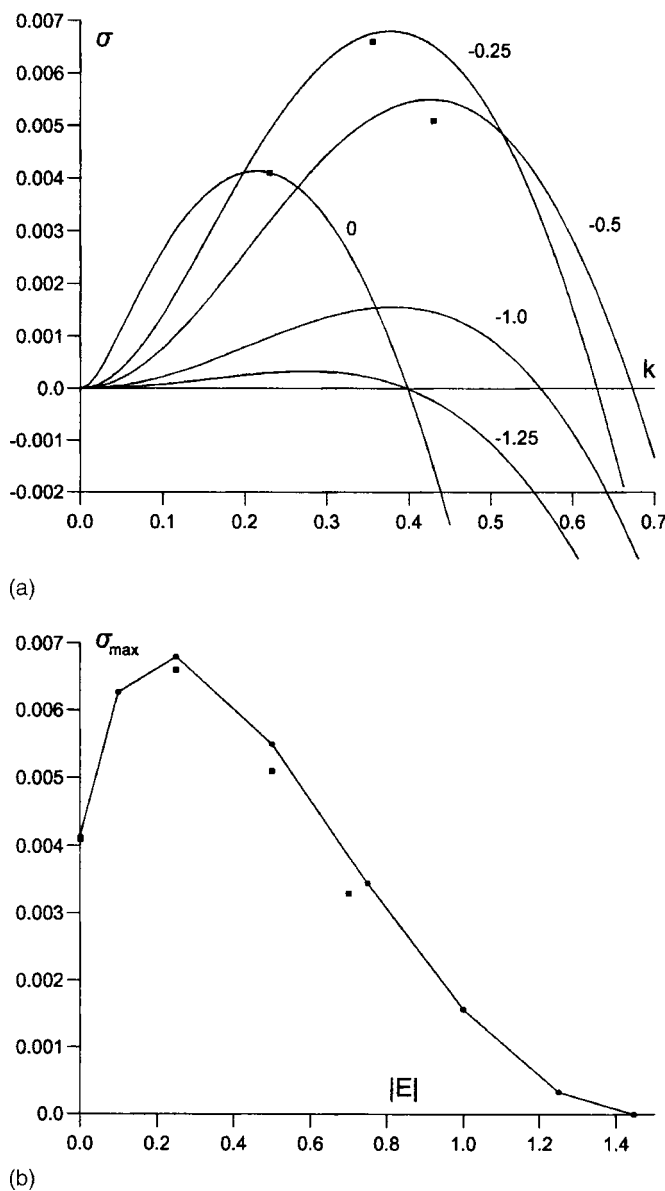
$$a(\zeta,y,t)=a(\zeta)+A(\zeta,y,t), \quad b(\zeta,y,t)=b(\zeta)+B(\zeta,y,t),$$
$$(9)$$

where A and B are assumed to be small. Applying Eq. (9) in Eqs. (3) and (4) and retaining only the leading order terms in A and B lead to the equations for our LSA as

$$\frac{\partial^2 A}{\partial \zeta^2}+\frac{\partial^2 A}{\partial y^2}+(c-E)\frac{\partial A}{\partial \zeta}-b^2 A-2abB=\frac{\partial A}{\partial t}, \quad (10)$$

$$D\left(\frac{\partial^2 B}{\partial \zeta^2}+\frac{\partial^2 B}{\partial y^2}\right)+(c-DE)\frac{\partial B}{\partial \zeta}+b^2 A+2abB=\frac{\partial B}{\partial t}. \quad (11)$$

We now look for a solution of Eqs. (10) and (11) in the form

$$A(\zeta,y,t)=e^{\sigma t+iky}A_0(\zeta), \quad B(\zeta,y,t)=e^{\sigma t+iky}B_0(\zeta). \quad (12)$$

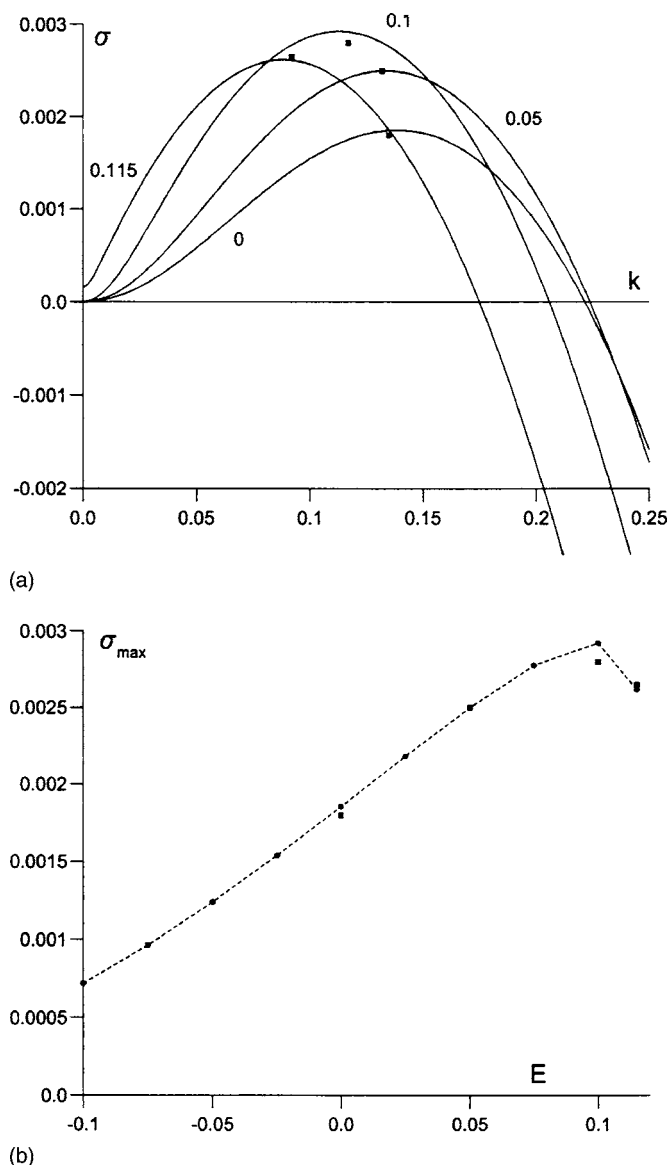This leads to the eigenvalue problem for $(A_0(\zeta),B_0(\zeta))$ as

(a)

(b)

FIG. 4. (a) Dispersion curves (plots of σ against k) obtained from a numerical solution of Eqs. (13) and (14), for $D=0.3$ and $E=0.0$, 0.05, 0.1, 0.115, (b) σ_{max}, the maximum value of the growth rate σ, plotted against E for $D=0.3$. Values of σ_{max} and k_{max} obtained from the integrations of Eqs. (3) and (4) are shown by ■.

$$A_0'' + (c-E)A_0' - (\sigma + k^2 + b^2)A_0 - 2abB_0 = 0, \qquad (13)$$

$$DB_0'' + (c-DE)B_0' - (\sigma + Dk^2 - 2ab)B_0 + b^2A_0 = 0, \quad (14)$$

in terms of the (linear) growth rate σ and the wave number k, with $\sigma = \sigma(k)$, subject to

$$A_0 \to 0, \quad B_0 \to 0 \quad \text{as} \quad \zeta \to \pm \infty. \qquad (15)$$

We note in passing that, when $D=1$, $a+b \equiv 1$, $c-E = 1/\sqrt{2}$, and that there is an analytic solution for $a(\zeta)$ and $b(\zeta)$.[14,17] From this it follows that, for the LSA, $A_0 + B_0 \equiv 0$ and that $\sigma = -k^2$, with the front being stable for all values of E. Thus, to obtain a diffusive instability even in the presence of an electric field, we require $D \neq 1$.

We obtained dispersion curves, plots of σ against k for given values of D and E, by solving Eqs. (13) and (14) numerically by a shooting method. This approach required

the solution to the traveling wave Eqs. (5) and (6) [as given in Fig. 2(a)] and built in the asymptotic forms for the solution as $\zeta \to \pm \infty$ resulting from Eq. (15). One of the arbitrary constants that appear in this development is being set to unity to force a nontrivial solution. The resulting (linear) boundary-value problem was solved using a standard shooting method (D02AGF in the NAG library). This method converged easily and enabled the dispersion curves to be readily calculated.

Results for $D=0.1$ are shown in Fig. 3(a) for a range of (negative) field strengths to compare with the field-free $E=0$ case. For this value of D, traveling waves exist for only very small positive field strengths, with the upper bound on E for the existence of a traveling wave being $E_c=0.0321$.[3] Figure 3(a) shows that small negative fields make the system more unstable, having higher growth rates and a wider range of unstable wave numbers. This can be seen, for example, by comparing the dispersion curves for $E=0.0$ and $E=-0.5$ in Fig. 3(a) and more clearly in Fig. 3(b), where we plot σ_{max}, the maximum value of σ obtained from these dispersion curve calculations, against $|E|$. Figure 3(b) shows that σ_{max} achieves its greatest value at $E \simeq -0.25$ for $D=0.1$. The effect of increasing the field strength further is to make the system more stable, as in the curves for $E=-1.0$ and $E=-1.25$ (lower maximum growth rates). For a sufficiently large negative field the system becomes fully stable. Integration of Eqs. (13) and (14) with $E=-1.5$ gave $\sigma < 0$ for all $k > 0$.

We next considered a higher value for D, namely, $D=0.3$, which still made the system unstable in field-free conditions but which gave a greater range of positive field strengths for the existence of traveling waves, here $E_c \simeq 0.115$. Our aim now is to examine the influence of a positive field on the stability of a diffusionally unstable reaction front. Dispersion curves are shown in Fig. 4(a) for positive fields and values of σ_{max} are given in Fig. 4(b). These figures show that the system becomes more unstable in a positive field through higher growth rates, though the range of unstable wave numbers does not vary significantly. In negative fields the system becomes more stable with lower growth rates and becomes fully stable at a relatively low field strength. Calculations with $E=-0.25$ had $\sigma < 0$ for all $k > 0$.

For values of $D > D_c \simeq 0.424$ a planar reaction front is stable in field-free conditions. The results shown in Fig. 4 suggest that a sufficiently strong positive field might make the front unstable when $D > D_c$. To examine this point we took $D=0.5$ with some corresponding dispersion curves being shown in Fig. 5, note that $E_c \simeq 0.251$ for $D=0.5$. This figure clearly shows that a positive field does make the front unstable even when $D > D_c$, though this requires a field strength greater than $E \simeq 0.12$ (approximately). For field strengths smaller than this our LSA calculations show that the front remains fully stable.

Further information about how the electric field influences the LSA can be obtained from the solution for small k, as was seen for the field-free case.[3]

A. Solution for $k \ll 1$

Here we follow Ref. 3 and look for a solution of Eqs. (13) and (14) valid for $k \ll 1$ by expanding
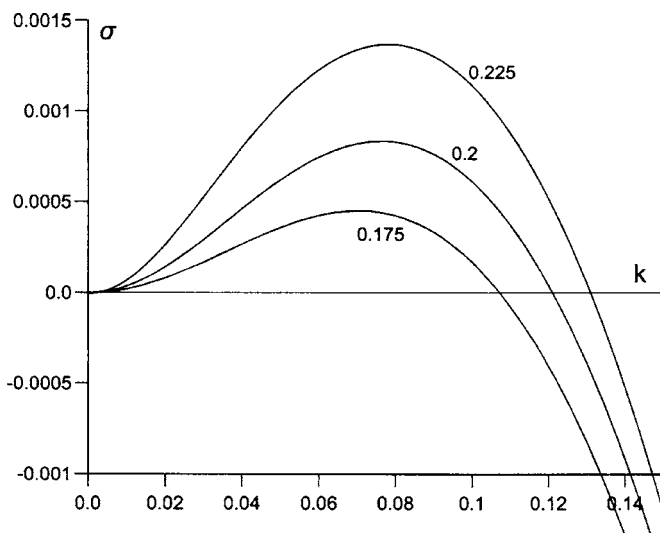
FIG. 5. Dispersion curves (plots of σ against k) obtained from a numerical solution of Eqs. (13) and (14), for $D=0.5$ and $E=0.175$, 0.2, and 0.225.

FIG. 6. Plots of σ_0, obtained from Eq. (24), against E for $D=0.1$, 0.2, 0.3, and 0.4 (diffusionally unstable for $E=0$) and for $D=0.5$ (diffusionally stable for $E=0$), $\sigma \sim \sigma_0 k^2$ for $k \ll 1$.

$$A_0(\zeta;k) = \widetilde{A}_0(\zeta) + \widetilde{A}_1(\zeta)k^2 + \cdots,$$

$$B_0(\zeta;k) = \widetilde{B}_0(\zeta) + \widetilde{B}_1(\zeta)k^2 + \dots, \tag{16}$$

with

$$\sigma(k) = \sigma_0 k^2 + \dots . \tag{17}$$

The leading order solution can be expressed in terms of the traveling wave solution as $\widetilde{A}_0 = a'$, $\widetilde{B}_0 = b'$. We can write the terms of $O(k^2)$ in the form

$$\frac{d}{d\zeta}(e^{v_1\zeta}\widetilde{A}_1') - (b^2\widetilde{A}_1 + 2ab\widetilde{B}_1)e^{v_1\zeta} = (\sigma_0 + 1)e^{v_1\zeta}a', \tag{18}$$

$$\frac{d}{d\zeta}(De^{v_2\zeta}\widetilde{B}_1') + (b^2\widetilde{A}_1 + 2ab\widetilde{B}_1)e^{v_2\zeta} = (\sigma_0 + D)e^{v_2\zeta}b', \tag{19}$$

where $v_1 = c - E$ and $v_2 = (c - DE)/D$ $(v_1 > 0, v_2 > 0)$ subject to the boundary conditions

$$\widetilde{A}_1 \rightarrow 0, \quad \widetilde{B}_1 \rightarrow 0 \quad \text{as} \quad \zeta \rightarrow \pm\infty. \tag{20}$$

Now Eqs. (18) and (19) have a solution (a', b') to the homogeneous problem which satisfies all the required boundary conditions. Thus, for the nonhomogeneous problem to have a solution again satisfying boundary conditions (20), the right-hand sides of Eqs. (18) and (19) must satisfy some compatibility condition. To determine this condition we construct the corresponding adjoint problem for $U(\zeta)$ and $V(\zeta)$, following directly from Ref. 3, as

$$\frac{d}{d\zeta}(e^{v_1\zeta}U') - b^2(e^{v_1\zeta}U - e^{v_2\zeta}V) = 0, \tag{21}$$

$$\frac{d}{d\zeta}(De^{v_2\zeta}V') - 2ab(e^{v_1\zeta}U - e^{v_2\zeta}V) = 0, \tag{22}$$

with

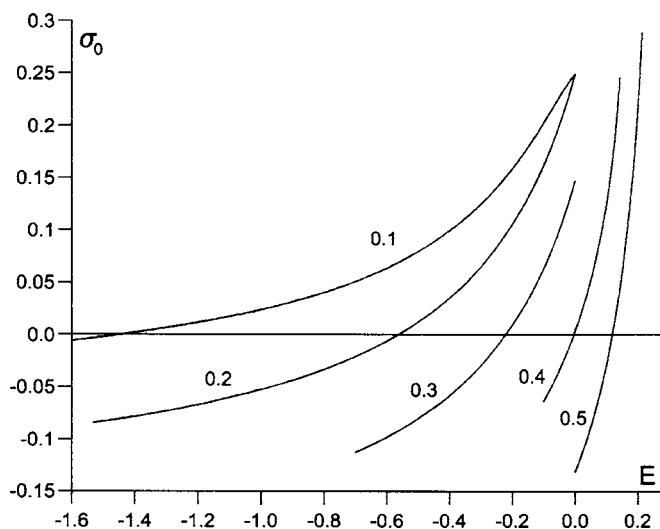$$U, V \rightarrow 0 \quad \text{as} \quad \zeta \rightarrow \pm\infty. \tag{23}$$

The compatibility condition is derived, again following Ref. 3, by multiplying Eq. (18) by $U(\zeta)$, Eq. (19) by $V(\zeta)$, and integrating. This gives the condition

$$(\sigma_0 + 1)\int_{-\infty}^{\infty} e^{v_1\zeta}a'Ud\zeta + (\sigma_0 + D)\int_{-\infty}^{\infty} e^{v_2\zeta}b'Vd\zeta = 0. \tag{24}$$

Equations (21)–(23) have to be solved numerically, which was done using the same approach as was used for the equations for the dispersion curves. Having determined $U(\zeta)$, $V(\zeta)$, these can be applied in the integrals and Eq. (24) then used to find σ_0, which will depend on both D and E. The system will be unstable, at least for some range of wave numbers, if $\sigma_0 > 0$.

Plots of σ_0 against E for a range of D, obtained from Eq. (24), are shown in Fig. 6. This figure shows that σ_0 is positive at $E=0$ for the values of $D < D_c$ plotted in the figure and that $\sigma_0 < 0$ at $E=0$ for $D=0.5 > D_c$, in line with the results given in Ref. 3. Note that, when $E=0$, $\sigma_0=0$ at $D=D_c$ $=0.4236$.[2,3] The values of σ_0 increase rapidly as E approaches the saddle-node bifurcation at E_c, where traveling wave solutions cease to exist. When $D < D_c$, the values of σ_0 decrease as the (negative) field strength is increased, consistent with Fig. 3(a). For $D=0.5$, σ_0 changes sign from negative to positive at a positive field strength $E \simeq 0.119$, with $\sigma_0 > 0$, and the reaction front then being unstable, for values of E greater than this. At some value E_0 of E (dependent on D) $\sigma_0=0$ and is negative for field strengths $E < E_0$. Values of E_0 obtained from our calculations for determining σ_0 are shown in Fig. 7. For small values of D, E_0 is negative and $|E_0|$ is relatively large. Note that, for $D=0.1$, $E_0=-1.447$, in agreement with the results shown in Fig. 3. The value of E_0 gets closer to $E=0$ as D is increased, as can be seen in Fig. 4. For example, for $D=0.4$, $\sigma_0=0$ at $E \simeq -0.0049$. For $D > D_c$, E_0 is positive with E_0 increasing as D increases from D_c.
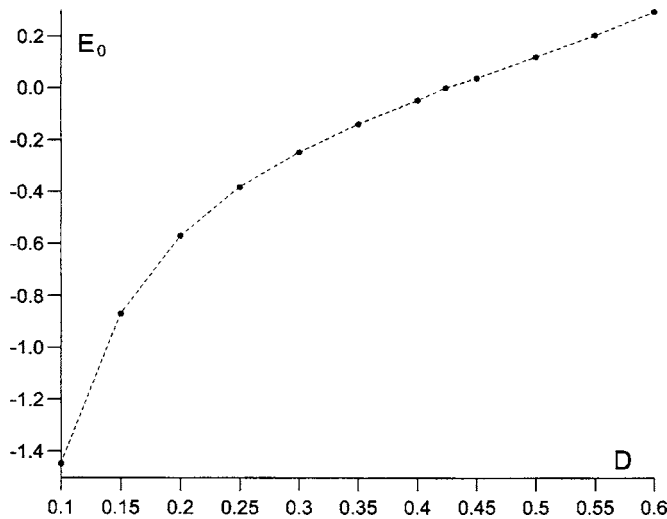
FIG. 7. The values of E_0, where $\sigma_0=0$, plotted against D.

The question remains as to whether there are sufficiently strong fields to make the front unstable as D is increased indefinitely. We find that this is not the case, with there being an upper bound on D for an instability. There is a trade-off between requiring a sufficiently large field strength to make the front unstable while having a small enough field strength for a traveling wave to exist, i.e., we need $E_c > E_0$ for an instability. We have already seen that $D=1$ is an upper bound; however, this appears not to be the limiting value for an instability. Our numerical calculations of σ_0 suggest that, when $D \simeq 0.81$, the values of E_0 and E_c are approximately the same, i.e., we need a value of D less than this for a traveling wave to exist which can be made unstable by applying an electric field. We summarize our results in Fig. 8, where we plot both E_0 and E_c to show the region (between the two curves) where, when $D > D_c$, traveling waves exist ($E < E_c$) and are unstable if a field of strength $E > E_0$ is applied.

V. BEHAVIOR NEAR THE TURNING POINTS

We have seen, for $D < 1$, that there is a positive upper bound E_c on E for the existence of a traveling wave solution [Fig. 2(a)] with two solution branches for $0 < E < E_c$.[14,17] We now examine the nature of the solution to the traveling wave Eqs. (5) when $|E - E_c| \ll 1$ and the consequences for the LSA. We set
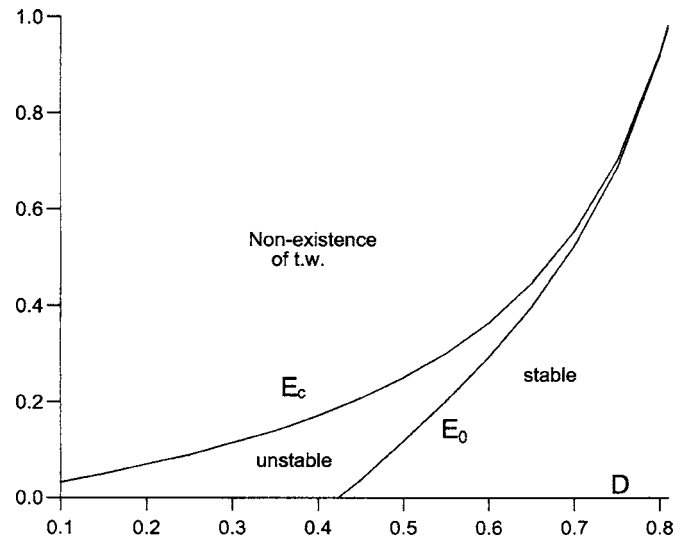
$$E = E_c - \delta, \quad 0 < \delta \ll 1, \tag{25}$$

and look for a solution of Eqs. (5) and (6) valid for δ small by expanding

$$c = c_0 + c_1 \delta^{1/2} + c_2 \delta + \dots,$$

$$a(\zeta; \delta) = a_0(\zeta) + c_1 a_1(\zeta) \delta^{1/2} + a_2(\zeta) \delta + \dots, \tag{26}$$

$$b(\zeta; \delta) = b_0(\zeta) + c_1 b_1(\zeta) \delta^{1/2} + b_2(\zeta) \delta + \dots.$$

The leading order problem for (a_0, b_0) is given by Eqs. (5) and (6) with E and c replaced by E_c and c_0, respectively. The corresponding value for b_s is given by Eq. (8).

At $O(\delta^{1/2})$ we have the linear problem

FIG. 8. Plots of E_c and E_0 against D to show the region where traveling waves exist ($E < E_c$) and are unstable if a field of strength $E > E_0$ is applied.

$$a_1'' + (c_0 - E_c)a_1' - (b_0^2 a_1 + 2a_0 b_0 b_1) = -a_0',$$

$$Db_1'' + (c_0 - DE_c)b_1' + (b_0^2 a_1 + 2a_0 b_0 b_1) = -b_0', \tag{27}$$

subject to

$$a_1 \to 0, \quad b_1 \to 0 \quad \text{as} \quad \zeta \to \infty,$$

$$a_1 \to 0, \quad b_1 \to -\frac{(D-1)E_c}{(c_0 - DE_c)^2} \quad \text{as} \quad \zeta \to -\infty. \tag{28}$$

The equations for (a_1, b_1) are essentially the same as those that arose in the small wave number analysis [Eqs. (18) and (19)]. We notice, as before, that these equations have a complementary function (a_0', b_0') that satisfies homogeneous boundary conditions. This leads to a compatibility condition and to construct this we use the adjoint problem given by Eqs. (21) and (22), with E now replaced by E_c. The resulting condition [see expression (24)] is that

$$I_1(E_c) + I_2(E_c) = 0, \tag{29}$$

where

$$I_1(E_c) = \int_{-\infty}^{\infty} e^{v_1 \zeta} a_0' U d\zeta, \quad I_2(E_c) = \int_{-\infty}^{\infty} e^{v_2 \zeta} b_0' V d\zeta,$$

and where we have now set $v_1 = c_0 - E_c$, $v_2 = (c_0 - DE_c)/D$.

It is condition (29), taken with the traveling wave Eqs. (5) and (6), that fixes E_c, as well as c_0. As a check, we examined the values of $I_1(E) + I_2(E)$ obtained from the small wave number analysis (for the construction of Fig. 6) and found that $I_1(E) + I_2(E) \to 0$ as the turning points, $E \to E_c$, in the $c \sim E$ curves were approached.

The equations at $O(\delta)$ are

$$a_2'' + (c_0 - E_c)a_2' - (b_0^2 a_2 + 2a_0 b_0 b_2)$$
$$= -(1 + c_2)a_0' + c_1^2 a_1' + c_1^2(a_0 b_1^2 + 2b_0 a_1 b_1),$$
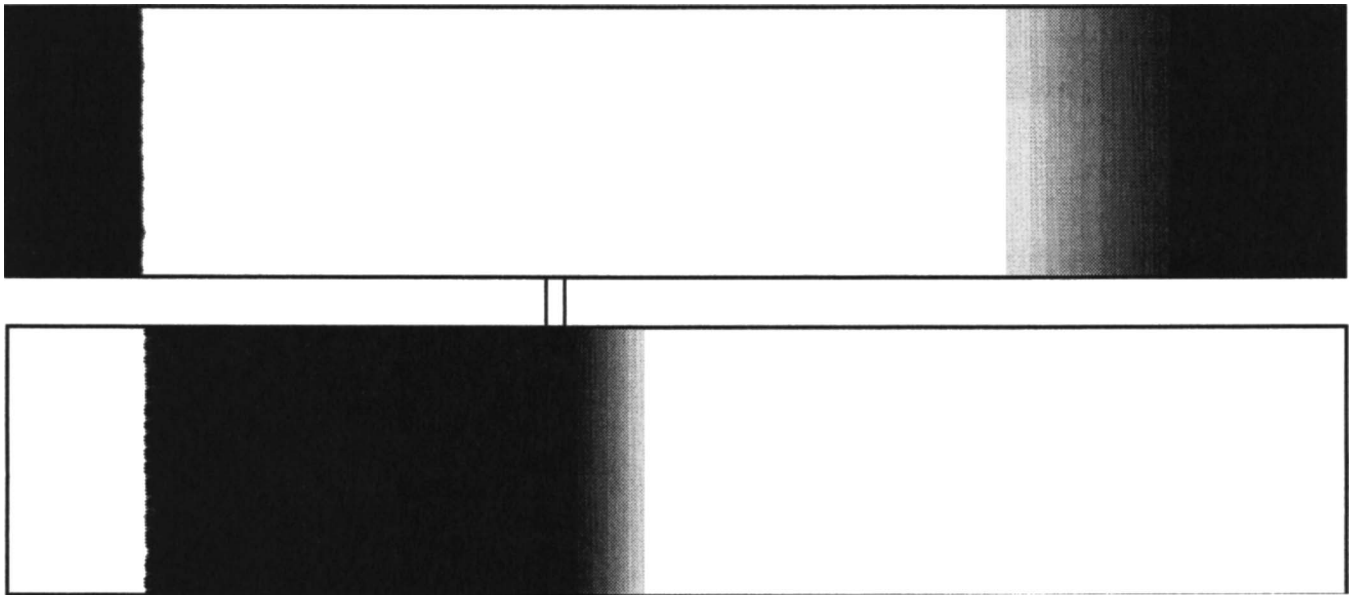
FIG. 9. Nonlinear simulation for $D=0.1$ and $|E|=0.25$ shown at time $t=2400$, the nondimensional width and length are 300 and 1500, respectively. The vertical lines indicate the positions where the fronts were initiated. The upper and lower panels represent a and b, respectively.

$$Db_2'' + (c_0 - DE_c)b_2' + (b_0^2 a_2 + 2a_0 b_0 b_2)$$
$$= -(c_2 + D)b_0' + c_1^2 b_1' - c_1^2(a_0 b_1^2 + 2b_0 a_1 b_1). \qquad (30)$$

The compatibility condition arising from Eqs. (30) gives, with Eq. (29),

$$c_1^2 = \frac{(1-D)I_1(E_c)}{I_3(E_c) + I_4(E_c)} \quad (D \neq 1), \qquad (31)$$

where

$$I_3(E_c) = \int_{-\infty}^{\infty} (a_1' U e^{v_1 \zeta} + b_1' V e^{v_2 \zeta}) d\zeta,$$

$$I_4(E_c) = \int_{-\infty}^{\infty} (a_0 b_1^2 + 2b_0 a_1 b_1)(U e^{v_1 \zeta} - V e^{v_2 \zeta}) d\zeta.$$

Expression (31) shows the emergence of two solution branches at $E=E_c$ from the $\pm$ signs on taking the square root.

We now examine the consequences for the LSA. We have seen that the analysis for small k, in particular, whether σ_0 is positive or negative, can determine the overall (linear) stability of the system. Now σ_0 is found from expression (24), which we can write as

$$\sigma_0 = -\frac{(I_1 + DI_2)}{(I_1 + I_2)}, \qquad (32)$$

where I_1 and I_2 are as defined above but now for a general field $E < E_c$. At $E = E_c$, the denominator in Eq. (32) is zero from Eq. (29), and, for $D \neq 1$, the numerator remains non-
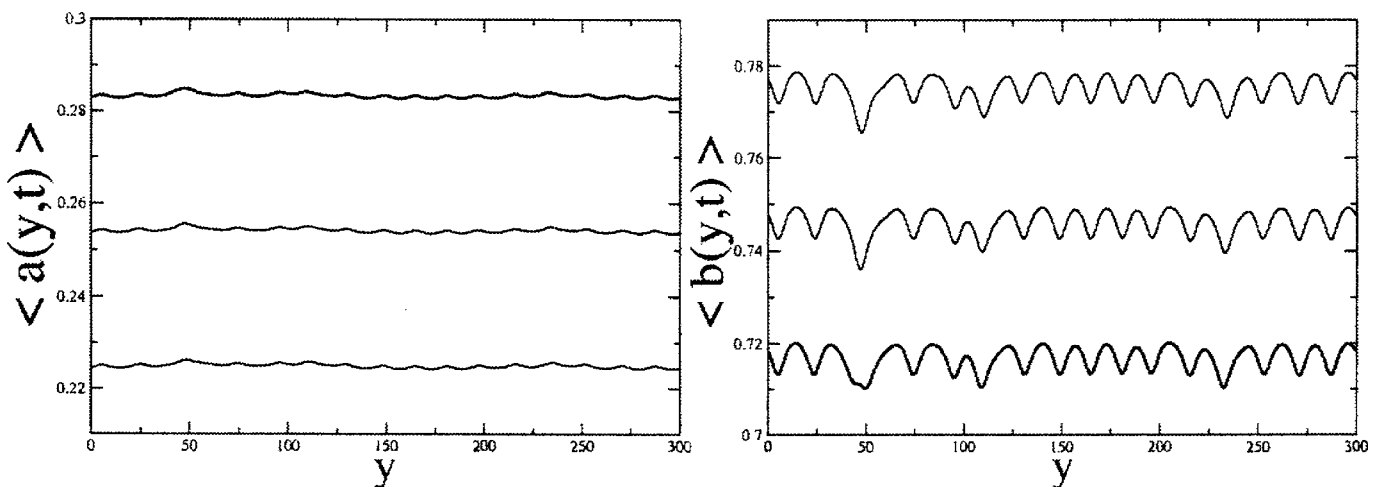

FIG. 10. Average transverse concentration profiles for a and b as a function of y, $D=0.1$ and $E=-0.25$. The bold line corresponds to the concentration shown at time $t=2400$, and the two other ones are taken at $t=2500$ and 2600, respectively.
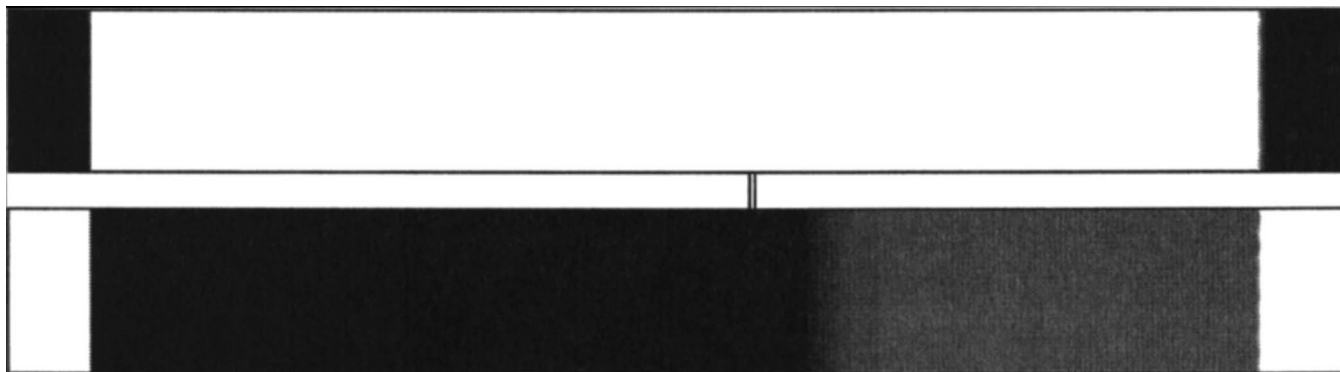
FIG. 11. Nonlinear simulation for $D=0.3$ and $|E|=0.1$ taken at time $t=4000$, the nondimensional width and length are 300 and 2500, respectively. The vertical lines indicate the positions where the fronts were initiated. The upper and lower panels represent a and b, respectively.

zero. Thus σ_0 becomes unbounded as $E \rightarrow E_c$, as can be seen in Fig. 6. Also, as the integrals I_1 and I_2 are smooth in E, having I_1+I_2 pass through zero means, from Eq. (32), that σ_0 will change sign at $E=E_c$ from the upper to the lower branch. This indicates that the lower branch could be transversely stable when the upper branch is unstable. However, these lower branch solutions appear to be longitudinally unstable, as is seen in one-dimensional numerical simulations of the corresponding reaction-diffusion problem.

Furthermore, condition (29) makes the $O(k^2)$ problem [Eqs. (18) and (19)] in the small k analysis degenerate. This requires a modification to the expansion at E_c to an expansion in powers of k (rather than previously in k^2), with now

$$\sigma = \omega_0 k + \omega_1 k^2 + \ldots , \tag{33}$$

and corresponding expansions for A_0 and B_0. The leading order problem still has the solution (a_0', b_0'). At $O(k)$ we obtain essentially Eqs. (27) with now the factor ω_0 multiplying the right-hand sides. From Eq. (27) the compatibility condition [analogous to Eq. (24)] is satisfied identically. At $O(k^2)$ we have

$$\tilde{A}_2'' + (c_0 - E_c)\tilde{A}_2' - b_0^2 \tilde{A}_2 - 2a_0 b_0 \tilde{B}_2 = \omega_0 \tilde{A}_1 + (\omega_1 + 1)a_0' ,$$

$$D\tilde{B}_2'' + (c_0 - DE_c)\tilde{B}_2' + b_0^2 \tilde{A}_2 + 2a_0 b_0 \tilde{B}_2$$

$$= \omega_0 \tilde{B}_1 + (\omega_1 + D)b_0' . \tag{34}$$

It is this problem that determines ω_0, the compatibility condition at this stage giving, on using Eq. (29),

$$\omega_0 I_5(E_c) + I_1(E_c) + DI_2(E_c) = 0 , \tag{35}$$

where

$$I_5(E_c) = \int_{-\infty}^{\infty} (\tilde{A}_1 U e^{v_1 \zeta} + \tilde{B}_1 V e^{v_2 \zeta}) d\zeta .$$

VI. NUMERICAL SIMULATIONS

Equations (3) and (4) were solved numerically using an explicit second-order finite-difference method along with a fourth-order Runge-Kutta scheme. We integrated the equations on a domain of width L_y and length L_x with no-flux boundary conditions applied along both the x and y directions. The simulations were started using as initial conditions a small rectangle of products for which $(a,b)=(0,1)$ embedded in a bulk of fresh reactant where $(a,b)=(1,0)$ with an intermediate line where the concentration is $a=b=1/2$ modified with a random noise of 0.1% amplitude. We checked the
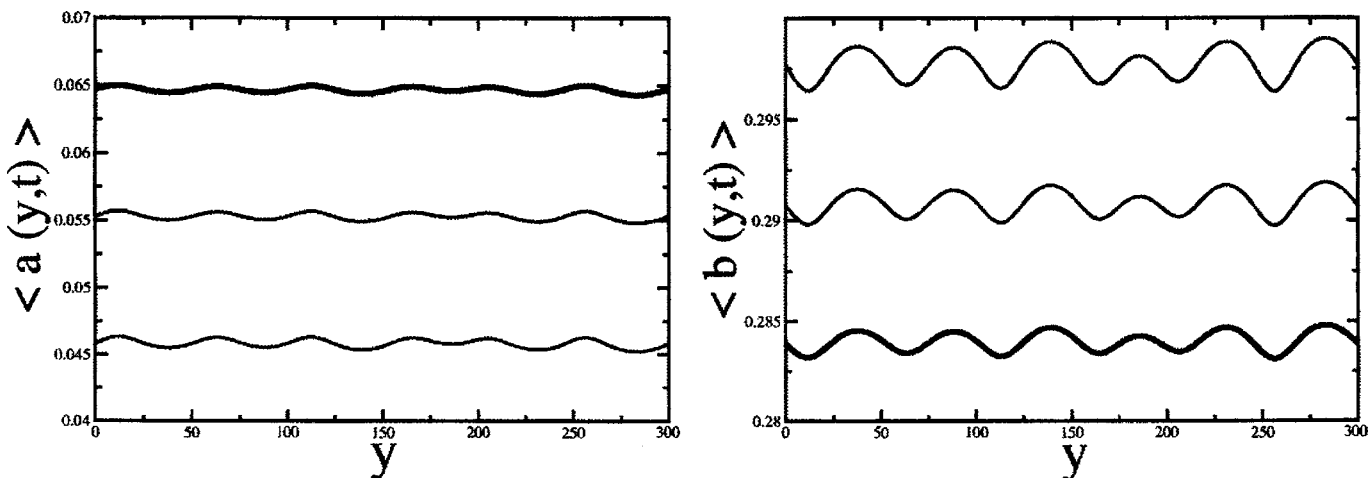

FIG. 12. Average transverse concentration profiles as a function of y for a and b with $D=0.3$ and $E=+0.1$. The bold line corresponds to the concentration shown at time $t=4000$, and the two other ones are taken at $t=4100$ and 4200, respectively.
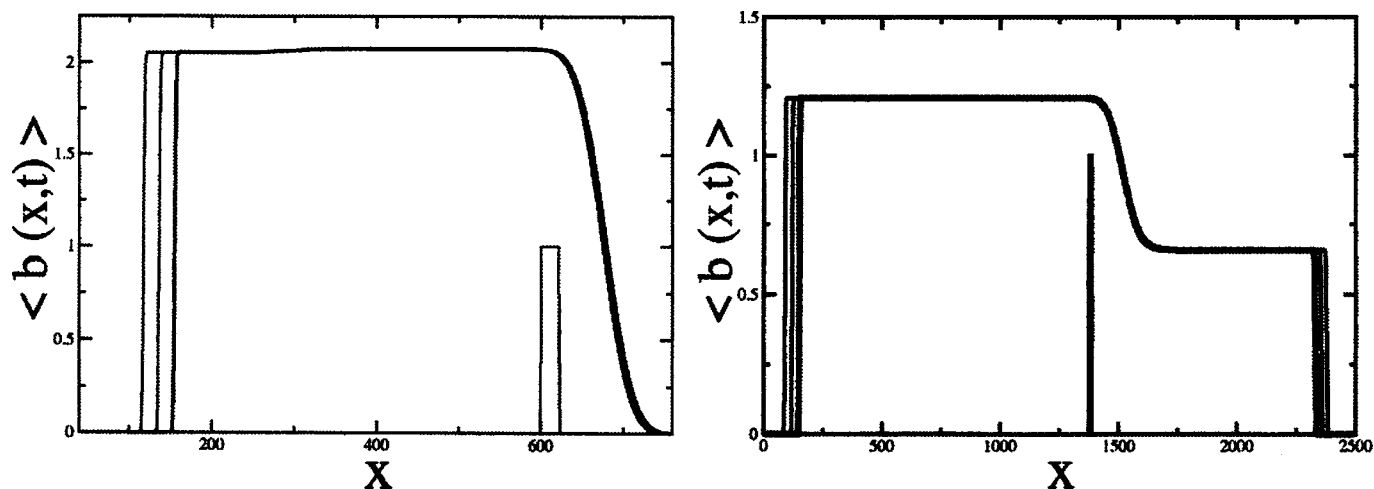
FIG. 13. Average longitudinal concentration profiles for b as a function of x. On the left $D=0.1$ and $|E|=0.25$, at times $t=0, 2400$ (bold), 2500, and 2600. On the right $D=0.3$ and $|E|=0.1$ at times $t=0, 4000$, (bold), 4100, and 4200.

precision of the code, refining the space and time steps as necessary. Typical values of effective spatial discretization steps were $\Delta x = \Delta y = 0.5$ while for the time discretization step we take $\Delta t = 0.01$. We checked that, for different values of D and E, we recover the reaction-diffusion speed of diffusively stable fronts as well as the electrophoretic separation between a and b. The concentration fields are visualized on a gray scale ranging from white for $a = b = 0$ to black for $a = 1$ and $b = b_s$, respectively.

Numerical simulations were first performed for $D = 0.1$ and for various field strengths. These calculations confirmed the general conclusions obtained from the LSA. From these results we were able to estimate the growth rate from the initial development of the instability, in effect $\sigma_{\max}$, with these values also being plotted in Fig. 3(b) (shown by ■). There is good agreement with the values determined from the LSA, again acting as confirmation for our stability analysis. To compute these most unstable growth rates, we follow during time the average transverse concentration profiles defined as $\langle b(y,t)\rangle = (1/L_x)\int_0^{L_x} b(x,y,t)dx$ for b, with a similar definition for a. We then Fourier transform this profile and identify the most unstable wave number as the one with the largest power in the Fourier spectrum. At early times, the amplitude A of the modes grows exponentially. The growth rate of the most unstable mode is then obtained as a linear fit to the curve $\log A$ as a function of time. The related most unstable wave numbers $k = k_{\max}$ and growth rates $\sigma_{\max}$ are plotted in Figs. 3(a) and 4(a) (shown by ■). Good agreement between the cellular properties of the front predicted by the LSA and those observed numerically is obtained in both cases. In the same spirit, we have checked that, for $D = 0.1$ and $E < -1.5$, any noise even of large amplitude added initially to the planar front decreases in time, confirming the stability predicted in Fig. 3(b).

To illustrate the nonlinear dynamics, Fig. 9 shows the effect of an electric field $|E| = 0.25$ on the diffusional instability for $D = 0.1$. The initial location of the two counter-propagating fronts is given by the two bars in between the upper and lower figures representing a and b, respectively. The front propagating to the right feels a positive electric

field E while the one traveling to the left evolves in the equivalent of a negative electric field $-E$ of the same magnitude. Hence one nonlinear simulation with two counter-propagating fronts allows us to visualize at the same time the effect of positive and negative electric fields of the same magnitude for a given value of D. We see in Fig. 9 that for $D = 0.1$ and $E = +0.25$, the effect of a positive field is to lead to an electrophoretic separation between a and b with no diffusive instability. This is consistent with Fig. 2(b) showing that these values of D and E correspond to a point above the upper bound for the existence of traveling waves. The front propagating to the left feels a negative field $E = -0.25$ for which a traveling front exists and is diffusively unstable. This features a regular cellular structure, the wavelength of which is in agreement with the linear stability analysis shown in Fig. 3(b). The stationary character of the diffusively unstable structure can be appreciated from Fig. 10 which represents the average transverse concentration profiles for a and b from $t = 2400$ to $t = 2600$, with time $t = 2400$ shown in bold.

For some other values of the parameters, both the fronts propagating to the right and to the left give traveling waves and no electrophoretic separation. This is the case, for example, with $D = 0.3$ and $|E| = 0.1$, as shown in Fig. 11, where we see that on both sides the fronts travel as reaction-diffusion fronts. The one on the right feels a positive electric field and is in the region of existence of traveling waves. It is moreover diffusionally unstable and develops a cellular pattern with a wavelength $\lambda = 50$ (see Fig. 12), i.e., a most unstable wave number $k_{\max} = 0.126$ in good agreement with the linear stability analysis. The front propagating to the left in a negative electric field is stable.

Figure 13 shows the average longitudinal concentration profile of b defined as $\langle b(x,t)\rangle = (1/L_y)\int_0^{L_y} b(x,y,t)dy$ for the values of the parameters used for Figs. 9 and 11, respectively. We see here that, starting from an initial small reacted zone where b is set equal to 1, the front evolves in the presence of an electric field to a fully reacted concentration b_s larger than unity and given by Eq. (8) for a given propagation speed c. As an example for $D = 0.1$ and $E = -0.25$ (left

part of Fig. 13), we have $c=0.187$ (Ref. 17) which gives b_s $=2.06$ for both a and b traveling together to the left. In a positive electric field $E=+0.25$ the electrophoretic separation occurs and a travels at speed $c=|E|=0.25$ while b travels slower at a speed $c=D|E|=0.025$. For $D=0.3$ and $|E|=0.1$ (right part of Fig. 13), the predicted front propagation speed for the front traveling to the right in a positive E is c $=0.235$ which gives a concentration $b_s=0.658$ also in line with the nonlinear simulation obtained values of $c=0.234$ and $b_s=0.66$.

VII. CONCLUSIONS

We have shown that applying a constant electric field in the direction of propagation can change the stability characteristics of reaction-diffusion (RD) fronts. We have considered the specific case of a cubic autocatalytic reaction in which both the reactants have the same (negative) ionic charge. We have analyzed the influence on the diffusive instabilities of RD fronts in this system of an applied electric field in terms of two parameters, namely, the intensity E of the applied field and D the ratio of diffusion coefficients of the two important chemical species. Our main conclusions for this case are that if the RD front is diffusionally stable in field-free conditions, then there is a sufficiently strong positive field that can make the front transversely unstable. Conversely, we find that if the RD front is diffusionally unstable in field-free conditions, then a sufficiently strong negative field can make it stable.

We find good agreement between the predictions of a linear stability analysis and the corresponding numerical simulations of the full nonlinear model. Consequently, the results obtained from the LSA for the present configuration are a very good indicator of the behavior of the full nonlinear model. Moreover, since the dispersion curves calculated from the LSA have a "parabolic" appearance [see Figs. 3(a), 4(a), and 5], the calculation of σ_0 in the small wave number asymptotics [as in Eq. (24)] can fully determine whether the system is stable or not, though this calculation does not give the most unstable wave number or the corresponding maximum growth rate.

We have predicted the values of E_c, the upper bound on E for the existence of traveling waves for our model as well as E_0, the lower bound on E for diffusive instabilities of the front, both as functions of D. This then gives, in the (E,D) parameter space, the location of existence of diffusive instabilities affected by electric fields, as summarized in Fig. 8.

Qualitatively similar behavior was reported in Ref. 10 for a case when the chemical species had opposite ionic charges, showing, as in Fig. 8, parameter regions where there are stable fronts, lateral instabilities, and nonexistence of traveling wave solutions. There are differences between this case and ours, in that Tóth *et al.*[10] report that reaction fronts can exist and can be unstable for increasingly greater values of E as the parameter D (in our notation) is decreased. The opposite is true in our case, see Fig. 8. Tóth *et al.*[10] also give results for a case when both reactant species have ionic charges of the same sign, with that of B being twice that of A. For this case they find essentially the same behavior, as is seen in Fig. 8, except that they find two disjoint regions of (E,D) parameter space for $D<1$ where the reaction front is unstable. This is not seen in our case, where the ionic charges are the same.

[1] D. Horváth, V. Petrov, S. K. Scott, and K. Showalter, J. Chem. Phys. **98**, 6332 (1993).
[2] A. Malevanets, A. Careta, and R. Kapral, Phys. Rev. E **52**, 4724 (1995).
[3] J. H. Merkin and I. Z. Kiss, Phys. Rev. E **72**, 026219 (2005).
[4] J. H. Merkin and H. Ševčíková, Phys. Chem. Chem. Phys. **1**, 91 (1999).
[5] D. Horváth and K. Showalter, J. Chem. Phys. **102**, 2471 (1995).
[6] A. Tóth, I. Lagzi, and D. Horváth, J. Phys. Chem. **100**, 14837 (1996).
[7] D. Horváth and A. Tóth, J. Chem. Phys. **108**, 1447 (1998).
[8] A. Tóth, B. Veisz, and D. Horváth, J. Phys. Chem. A **102**, 5157 (1998).
[9] M. Fuentes, M. N. Kuperman, and P. De Kepper, J. Phys. Chem. A **105**, 6769 (2001).
[10] A. Tóth, D. Horváth, and W. van Saarloos, J. Chem. Phys. **111**, 10964 (1999).
[11] D. Horváth, A. Tóth, and K. Yoshikawa, J. Chem. Phys. **111**, 10 (1999).
[12] Z. Virányi, A. Szommer, A. Tóth, and D. Horváth, Phys. Chem. Chem. Phys. **6**, 3396 (2004).
[13] J. H. Merkin, H. Ševčíková, D. Šnita, and M. Marek, IMA J. Appl. Math. **60**, 1 (1998).
[14] J. H. Merkin and H. Ševčíková, J. Math. Chem. **25**, 111 (1999).
[15] J. H. Merkin, H. Ševčíková, and D. Šnita, IMA J. Appl. Math. **64**, 157 (2000).
[16] A. Zadražil, I. Z. Kiss, J. D'Hernoncourt, H. Ševčíková, J. H. Merkin, and A. De Wit, Phys. Rev. E **71**, 026224 (2005).
[17] J. H. Merkin, J. Math. Chem. **38**, 657 (2005).